British Journal of Obstetrics and Gynaecology
October 1999, Vol 106, pp. 1071–1077

NEW TECHNIQUES

High resolution imaging of endometriosis and ovarian carcinoma with optical coherence tomography: feasibility for laparoscopic-based imaging

*†**S. A. Boppart** *Research Affiliate,* ‡**A. Goodman** *Gynaecologist,* §**J. Libus** *Technician,* *†**C. Pitris** *Research Assistant,* ***C. A. Jesser** *Technician,* ‡**M. E. Brezinski** *Assistant Professor,* ***J. G. Fujimoto** *Professor*

**Department of Electrical Engineering and Computer Science, Research Laboratory of Electronics; †Havard-MIT Division of Health Sciences and Technology, Massachusetts Institute of Technology, Cambridge, Massachusetts; ‡Massachusetts General Hospital, Harvard Medical School, Boston, Massachusetts; §Department of Biology, King's College, Wilkes-Barre, Philadelphia, USA*

High resolution imaging of gynaecological tissue offers the potential for identifying pathological changes at early stages when interventions are more effective. Optical coherence tomography (OCT) is a high resolution high speed optical imaging technology which is analogous to ultrasound B-mode imaging except reflections of light are detected rather than sound. The OCT technology is capable of being integrated with laparoscopy for real-time subsurface imaging. In this report, the feasibility of OCT for differentiating normal and pathologic laparoscopically-accessible gynaecologic tissue is demonstrated. Differentiation is based on architectural changes of *in vitro* tissue morphology. OCT has the potential to improve conventional laparoscopy by enabling subsurface imaging near the level of histopathology.

Introduction

Imaging techniques such as magnetic resonance imaging[1–3], computed tomography[4], and clinical ultrasound[5,6], although powerful diagnostic technologies for a wide range of disorders, have maximum resolutions no greater than a few hundred microns. These resolutions are not suitable for detecting microstructural pathology such as early malignancies and endometriosis. Laparoscopic imaging provides a magnified look at tissue for diagnostic and surgical gynaecological procedures such as treating endometriosis[7], performing tubal ligation[8], managing benign ovarian cysts[9], and detecting persistent or recurrent malignant disease[10,11]. However, only surface features are visible with laparoscopy and, under many clinical scenarios, it would be of greater value to assess subsurface microstructure. A technology capable of imaging gynaecological tissue near the level of histopathology, in real-time, could be a powerful tool in the management of many gynaecological disorders. The ability to obtain an 'optical biopsy', a high-resolution, cross-sectional image of tissue *in situ*, without having to physically resect tissue, has the potential benefits of screening larger areas of tissue, directing the surgeon toward suspect sites for excisional biopsy, and reducing the time-delay of obtaining frozen sections by displaying images intraoperatively.

Optical coherence tomography (OCT) is a recently developed micron-scale real-time, imaging technology[12,13]. OCT is analogous to ultrasound, measuring the intensity of back-reflected infrared light rather than acoustical waves. OCT was first applied clinically to image and track retinal diseases in the transparent structures of the human eye[14]. Recently, OCT has been developed for imaging nontransparent tissues[15–17]. High speed OCT imaging has provided continuous feedback for guiding *in vitro* microsurgical anastomosis procedures[18] and has shown a feasibility for identifying brain tumour margins for neurosurgery[19]. *In vivo* imaging of the gastrointestinal and respiratory tracts has been performed in the rabbit using a 1 mm diameter catheter endoscope at four frames per second and 10 μm resolution[20].

Several features, in addition to high resolution, make OCT attractive for assessing gynaecological tissue. Firstly, OCT imaging is fiber based, allowing it to be readily integrated with hand-held probes, laparoscopes, catheters, and endoscopes[21]. Secondly, unlike ultrasound, OCT imaging does not require direct contact and can be performed through air. Thirdly, OCT systems are compact and portable, an important consideration for

Correspondence: Dr S. A. Boppart, Department of Electrical Engineering and Computer Science, Research Laboratory of Electronics, Massachusetts Institute of Technology, 77 Massachusetts Ave, Room 36–345, Cambridge, Massachusetts 02139, USA.

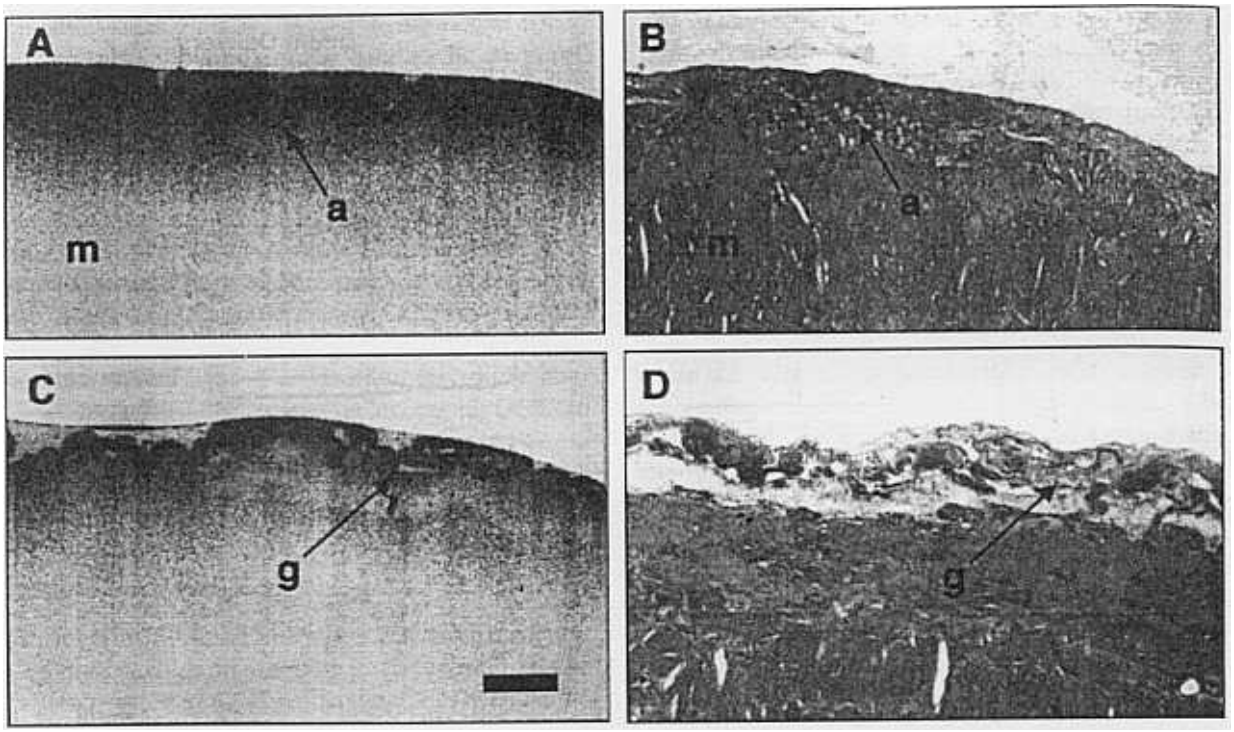

Fig. 2. Endometriosis on peritoneal surface of uterus. A, B) OCT image and corresponding histology of the peritoneal surface of normal uterus. This relatively homogeneous tissue is contrasted with C, D) endometriosis showing characteristic glandular structure. Tissue was imaged with an orientation consistent with *in vivo* laparoscopic exam. Abbreviations: a = adipose tissue; g = glandular morphology; m = uterine myometrium. Bar represents 1 mm.

optical absorption and scattering is observed with increasing depth. This normal region of uterus is contrasted with an adjacent endometriosis lesion. Increased glandular structure is observed in both the OCT image and histology (Fig. 2 C and 2 D, respectively). These characteristic glandular structures are present up to 1 mm below the peritoneal surface of the uterus.

The second pathologic gynaecological specimen is a primary serous papillary cystadenocarcinoma of the ovary which is contrasted with a region of normal ovary from the same patient. The normal ovary morphology is relatively uniform in both the OCT image (Fig. 3 A) and the corresponding histology (Fig. 3 B). The ovarian carcinoma in Figs 3 C and 3 D shows regions of cysts with surrounding regions of papillary structures. The larger cysts provide a contrast from the surrounding ovarian morphology. The serous fluid-filled cavities provide a lower backscattered optical signal because the fluid is more homogeneous and less scattering than the surrounding papillary structures. Similar observations are noted in the histopathology. The depth of imaging penetration in this ovary specimen is 2 mm, which is greater than in the uterine tissue.

The third gynaecologic pathology was imaged on a uterine specimen and shown in Fig. 4. The normal peritoneal surface of the uterus in Fig. 4 A and 4 B shows a region of serosal tissue adjacent to normal, relatively homogeneous, myometrium. This normal region is contrasted with a small region of ovarian adenoma which was suspected to have spread from the ovary due to an adhesion between the two organs. The neoplastic tissue is difficult to differentiate in the OCT image in Fig. 4 C due to the small dimensions of the glandular structures which are near the resolution limit of OCT. Using a calibrated reticule, measurements of gland dimensions were obtained from light microscopy of the histology. Glandular structures ranged in size of 5–25 μm, confirming their size near the resolution of the OCT system. The glandular spaces in the OCT image (Fig. 4 C) appear as subtle low-backscattering regions, but cannot be clearly resolved. Adjacent to the glandular tissue is an incidental finding of a small 1 × 2 mm subserosal leiomyoma. This region of dense smooth muscle is more clearly defined on the OCT image and confirmed in the corresponding histology in Fig. 4 D. Interestingly, the OCT image of the leiomyoma shows a central region of low optical backscatter (light gray) with a surrounding region of higher backscatter (dark gray). The corresponding histopathology reveals a relatively uniform structure. Depth of imaging in this uterus specimen is 2 mm.

Discussion

The ability to image and diagnose pathologic changes enables more effective treatment options and improved

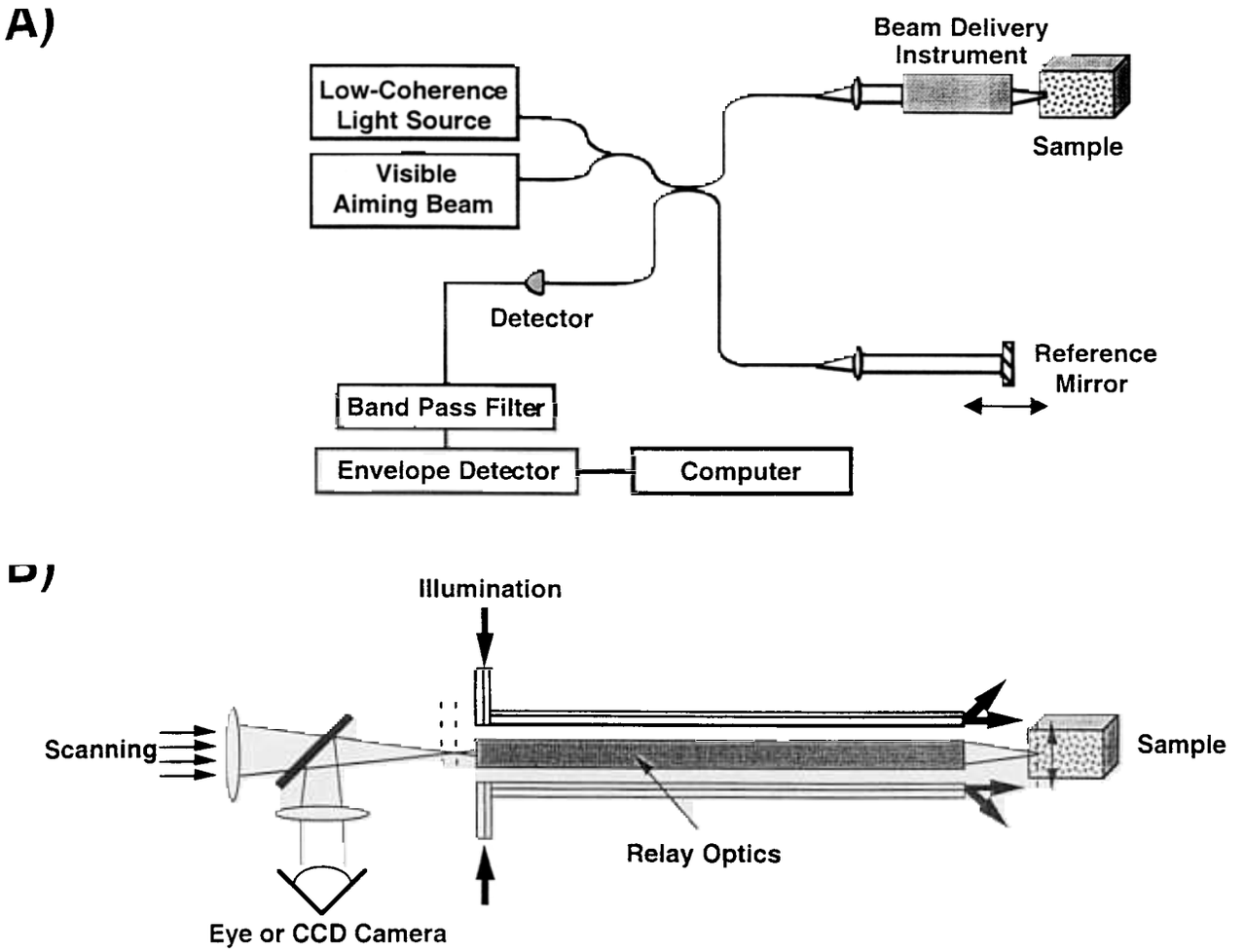

Fig. 1. Optical coherence tomography schematic. A) OCT uses a fiber-optic interferometer to localise optical backreflections from within tissue. Two-dimensional subsurface images are generated by scanning the beam across the tissue. B) The optic and fiber-based technology can be readily integrated into surgical instruments such as the laparoscope. Implementation permits simultaneous visualisation of surface features combined with subsurface OCT imaging.

the OCT imaging plane. The slices were embedded in paraffin wax. Histological sections, 5 μm thick, were sectioned along the OCT imaging plane and stained with hematoxylin and eosin for empiric comparison with acquired OCT images. Histological observations of subsurface tissue morphology were made using light microscopy.

Raw binary OCT data-arrays corresponding to the magnitude of optical backscatter from localised regions within the tissue were processed using Image 1·60 (National Institutes of Health, Bethesda, Maryland) on a Power Macintosh 9500/200 (Apple Computer Inc, Cupertino, California, USA). Processed gray-scale OCT images were analysed to determine the depth of imaging penetration, the presence of morphological features, and the similarities and differences between the imaged morphology and the morphology present in the corresponding histopathology. The protocol to use discarded tissue had been approved by the Committee on the Use of Human Subjects at Massachusetts General Hospital.

Results

Ninety OCT images and 30 histological sections were acquired from normal and pathologic sites on two uterus and one ovary specimens. Representative pairs of OCT images and corresponding histology are illustrated and described. An OCT image of normal uterus acquired from the peritoneal surface is shown in Fig. 2 A. Corresponding histology is shown in Fig. 2 B. The normal peritoneal surface of the uterus appears relatively homogeneous at these OCT image resolutions. Occasional invaginating structures along the surface, and subsurface collections of adipose tissue, are observed in both the OCT image and the corresponding histology. Imaging depth is limited to 1–1·5 mm and the exponential decrease in signal due to

the operating suite. Finally, OCT imaging is performed at high speeds, allowing image data to be acquired rapidly over large surface areas.

In this study high resolution OCT imaging of three *in vitro* human gynaecological pathologies is demonstrated: endometriosis, primary ovarian cancer, and metastatic ovarian cancer. Images of pathologic tissues are compared with those of normal tissues from the same subjects. Each pathological specimen was selected because of relevancy to future *in vivo* OCT imaging and was imaged in the orientation encountered during laparoscopic procedures. This preliminary study suggests the feasibility for using laparoscopic OCT to detect subsurface pathological changes.

Methods

Optical coherence tomography

Optical coherence tomography is a technique for performing high resolution imaging in biological tissue. The laboratory-based OCT instrument described here was constructed from commercially available optical components and previously described in detail[12,13]. This bench-top instrument has been used for the high resolution assessment of *in vitro* human tissue, including the cardiovascular[15], reproductive[17], and nervous[19] systems. OCT is analogous to ultrasound B-mode imaging except backscattering of light is detected, rather than sound. Whereas ultrasound pulse propagation and detection can be described in terms of time delays, the echo delay time of light returning to the OCT instrument from the tissue cannot be measured directly by electronic methods due to the high speeds associated with the propagation of light. Therefore, a technique known as interferometry is used. A schematic representation of the fiber optic-based Michelson interferometer, which allows measurements of precise depth and magnitude of each reflection, is shown in Fig. 1 A.

With Michelson interferometry, light is split equally by a fiber coupler (Gould Fiber Optics, Millersville, Maryland, USA) with half sent to a reference arm and half sent to a sample arm of the interferometer. Light reflects off the mirror (reference arm) and from within the sample. Reflections or backscatter from both arms are recombined by the fiber coupler and detected by a photodiode (New Focus Inc, Santa Clara, California). Interference of the light returning from the two arms only occurs when their optical path lengths are matched to within the coherence length of the light source. The coherence length can be envisioned as analogous to the pulse duration and is inversely proportional to the optical spectral bandwidth.

The axial resolution is determined by the coherence length of the source. Therefore, light sources with broad wavelength spectrums will enable high axial resolutions. Using a multiple quantum well semiconductor optical amplifier with a center wavelength of 1314 nm as a near-infrared light source (AFC Technologies Inc, Quebec, Canada), a free-space axial resolution of 18 μm was determined by using the standard technique of measuring the point spread function off of a mirror placed in the sample arm. The transverse resolution is determined by the spot size of the incident beam within the tissue. The spot size was 28 μm which yielded a 970 μm confocal parameter (depth of field). The confocal parameter for the beam was selected to closely match axial and transverse resolutions while maintaining a sufficient depth of field.

The signal:noise ratio was 115 dB using 5 mW of incident power on the specimen. For typical tissues, this sensitivity permits imaging to depths of 2–3 mm. A single axial scan was acquired for every sweep of the reference arm mirror. Images were generated by assembling adjacent axial scans to form a two-dimensional, cross-sectional image of the optical backscatter intensity from within the specimen. Image data was displayed in gray-scale as the logarithm of the backscattered intensity *versus* position. Acquisition time for each image was 30 s. Figure 1 B is a schematic representation showing OCT integration with a laparoscope[21]. This design permits simultaneous visualisation of surface features with subsurface OCT imaging of microstructure.

Specimen preparation and imaging

Two human uterus specimens and one ovary were obtained post-mortem from three cadavers, stored in 0·9% saline solution, and imaged within 24 h. Specimens were placed on computer-controlled micron-precision translational stages for imaging. The tissue surface to be imaged was positioned to permit the optical beam to be incident from above the specimen. Thirty cross-sectional OCT images (6×3 mm, 600×400 pixels) were obtained from the peritoneal surface of each specimen with the orientation consistent with that encountered during a laparoscopic examination. Immediately following image acquisition, the location of the image plane was marked with India ink for registration between OCT images and histology. The scan location of the invisible (1314 nm) infrared imaging beam was noted with the aid of a coincident visible (632 nm) aiming beam.

Histology and image analysis

Imaged specimens were placed in a 10% buffered solution of formaldehyde for standard histological preparation. The formalin-fixed specimens were cut into 5 mm thick slices in a plane parallel but not coincident with

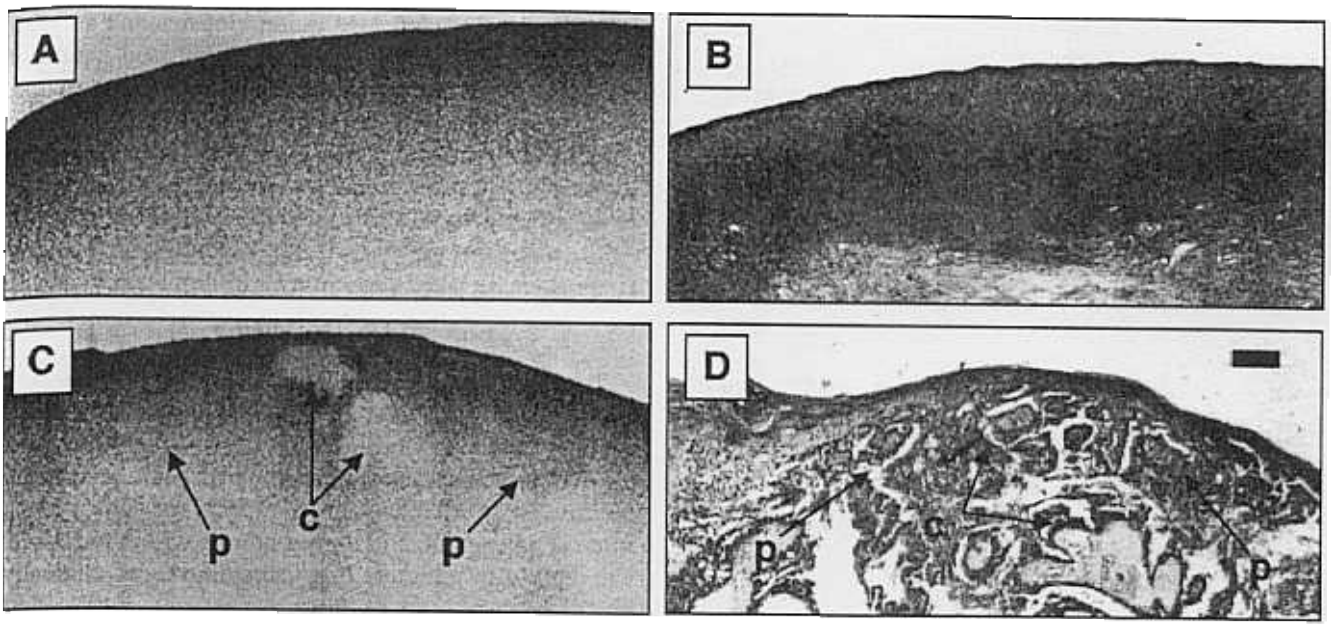

Fig. 3. Ovarian serous papillary cystadenocarcinoma. A, B) OCT image and corresponding histology of normal ovary. The OCT image of this normal specimen is relatively homogeneous compared with the presence of an C, D) ovarian carcinoma. Cysts containing serous fluid exhibit low-backscattering compared with the more highly backscattering cellular regions. Papillary structures surround the cysts. Abbreviations: c = cysts; P = papillary structures. Bar represents 1 mm.

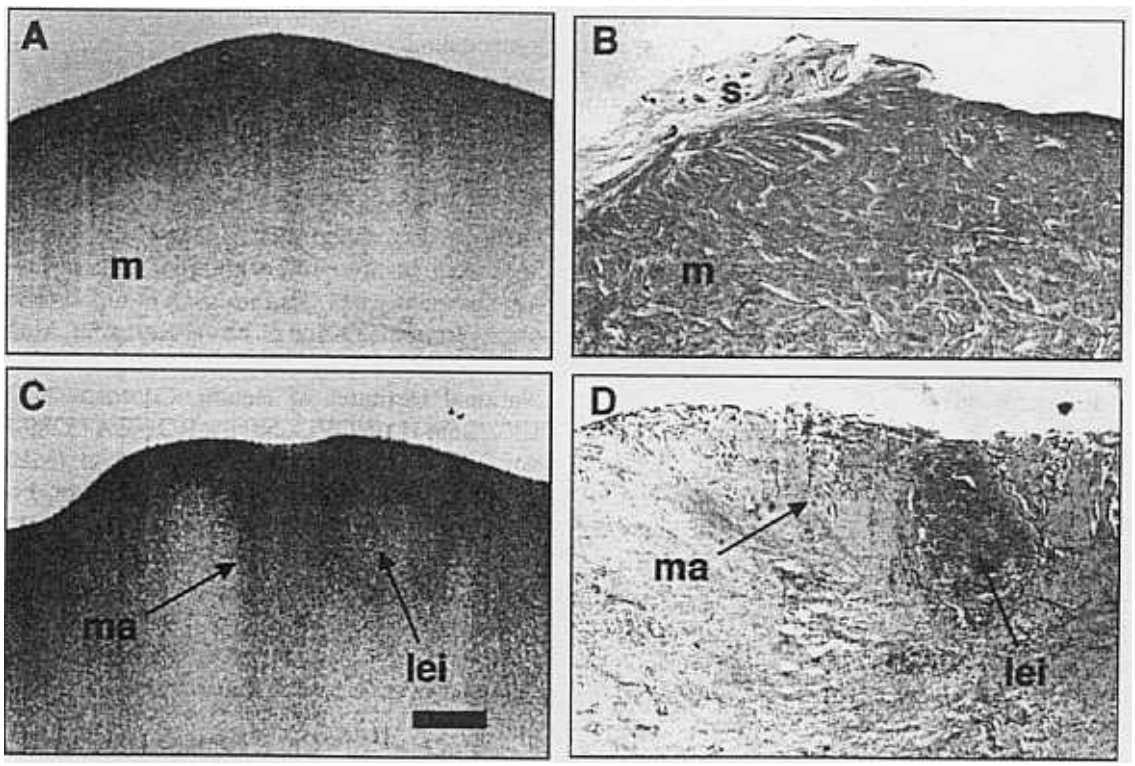

Fig. 4. Ovarian adenoma on uterus. A, B) OCT image and corresponding histology of a region of normal uterus for contrast with C, D) an ovarian adenoma which had spread to the peritoneal surface of the uterus following adhesion of the two organs. Small glandular morphology appears as localised regions of low and high backscatter in the OCT image. An incidental finding of a subserosal leiomyoma is apparent. Abbreviations: lei = leiomyoma; m = myometrium; ma = metastatic adenoma; s = serosal tissue. Bar represents 1 mm.

patient outcomes. Laparoscopy is one minimally invasive technique which enables diagnostic imaging and surgery to be performed with decreased morbidity. Although laparoscopy offers exceptional visualisation of remote, internal tissue, imaging is limited to surface features. In contrast, OCT enables cross-sectional, subsurface imaging of biological structures. The combination of these two techniques has the potential for improving the ability to sample suspect gynaecological tissue at high resolutions without excision. Subsurface high resolution OCT imaging of laparoscopically-accessible gynaecological tissue has been demonstrated in both normal and pathologic specimens. Acquired OCT images correlate well with corresponding histology, suggesting that OCT images can accurately represent the morphological tissue structure.

The image resolutions in this study permitted the definition of microscopic morphology and the differentiation between normal and abnormal gynaecological tissue. Resolutions, however, were not high enough to provide sharp images of small glands or individual cells. Because of this current resolution limitation, differentiation between abnormal benign and malignant tissue will be problematic and will require either improvements in image resolution or the identification of morphological features which are characteristic of malignancy. The axial and transverse resolutions in OCT are independent. The axial resolution is inversely proportional to the bandwidth of the optical source. Hence, larger spectral bandwidths can improve axial resolution. Axial resolutions as high as 1·9 μm have been achieved using broader bandwidth laser sources at shorter wavelengths[22,23]. Shorter wavelengths, however, are more highly absorbed and scattered in biological tissue, resulting in decreased imaging penetration. The transverse resolution is determined by the beam focusing optics. Higher transverse resolutions are possible, but at the expense of decreased depth of field. Individual cells and cellular processes, such as mitosis and migration, have been imaged *in vivo* with OCT in developmental biology animal models[24], but these differentiating cells were typically twice as large as cells found in normal human tissue. New laser sources and image processing techniques to permit cellular imaging, and to distinguish between abnormal benign and malignant human tissue, are currently under investigation.

Implementation of OCT for *in vivo* laparoscopic diagnostics will require faster acquisition rates and integration with surgical laparoscopic techniques. Although images in this feasibility study were acquired in 30 s, acquisition rates as high as eight frames per second have been achieved using a surgical microscope adapted for simultaneous OCT imaging[18]. Faster acquisition rates will be necessary to eliminate motion artifacts from both the patient and the operator, and to provide rapid feedback to guide biopsies and surgical procedures intraoperatively. The fiber-based nature of OCT can be implemented readily within a laparoscope, as shown in Fig. 1 B. However, special optics must be used to accommodate both the visible wavelengths of laparoscopy and the infrared wavelengths of OCT. The device must also be able to withstand repeated sterilisation. In the future there is the potential for spectroscopic imaging and detection to be implemented with laparoscopic OCT imaging because both techniques are optic-based and rely of fiber delivery systems[25,26].

These results are based on the empiric correlation between OCT images and histopathology of laparoscopically-accessible gynaecological tissue, and suggest that OCT can differentiate between normal and pathologic specimens. Differentiation is based on changes in microscopic architectural morphology within the tissue. The ability to integrate this technology with clinically useful devices, such as laparoscopes and endoscopes, suggests a feasibility for *in vivo* OCT imaging of subsurface morphology at near-histological resolutions. OCT imaging at real-time rates may also be used to guide biopsies and reduce sampling error. The use of OCT for the detection of pathological changes without having to physically resect and histologically prepare tissue may be a powerful diagnostic tool. Future studies should investigate laparoscopic-based OCT imaging in animal models for *in vivo* diagnostics of endometriosis and gynaecological malignancies.

Acknowledgements

The authors would like to thank Dr D. Stamper from King's College, Wilkes-Barre, Pennsylvania, for her technical assistance and Ms C. Kopf from the Massachusetts Institute of Technology for her aid in preparing this manuscript. This research is supported in part by grants from the Office of Naval Research, Medical Free Electron Laser Program, Grant N00014-97-1-1066, the National Institutes of Health, Contracts NIH-9-RO1-EY11289-11 (JGF), NIH-1-RO1-CA75289-01 (JGF and MEB), NIH-1-R29-HL55686-01A1 (MEB), NIH-RO1-AR44812-01 (MEB), the Whitaker Foundation Contract 96-0205 (MEB), the Air Force Office of Scientific Research, Grant F49620-95-1-0221, and the Air Force Palace Knight Program.

References

1 Shapiro I, Lanir A, Sharf M, Clouse ME, Lee RG. Magnetic resonance imaging of gynecologic masses. *Gynecol Oncol* 1987; **28**: 186–200.
2 Mitchell DG, Outwater EK. Benign gynecologic disease: applications of magnetic resonance imaging. *Top Magn Reson Imaging* 1995; 7: 26–43.
3 Troiano RN, Smith R. Malignant gynecologic disease: applications of magnetic resonance imaging. *Top Magn Reson Imaging* 1995; 7: 44–53.
4 King LA, Talledo OE, Gallup DG, el Gammal TA. Computed tomography in evaluation of gynecologic malignancies: a retrospective analysis. *Am J Obstet Gynecol* 1986; **155**: 960–964.

5 Granberg S, Wikland M. A comparison between ultrasound and gynecologic examination for detection of enlarged ovaries in a group of women at risk for ovarian carcinoma. *J Ultrasound Med* 1988; **7**: 59–64.
6 Andolf E, Jorgensen C. A prospective comparison of transabdominal and transvaginal ultrasound with surgical findings in gynecologic disease. *J Ultrasound Med* 1990; **9**: 71–75.
7 Mais V, Ajossa S, Guerriero S, Paoletti AM, Palmas M, Mascia M, Melis GB. The role of laparoscopy in the treatment of endometriosis. *Clin Exp Obstet Gynecol* 1994; **21**: 225–227.
8 Clark DH Jr, Schneider GT, McManus S. Tubal sterilization: comparison of outpatient laparoscopy and postpartum ligation. *J Reprod Med* 1974; **13**: 69–70.
9 Marana R, Caruana P, Muzil L, Catalano GF, Mancuso S. Operative laparoscopy for ovarian cysts. Excision vs. aspiration. *J Reprod Med* 1996; **41**: 435–438.
10 Amara DP, Nezhat C, Teng NN, Nezhat F, Nezhat C, Rosati M. Operative laparoscopy in the management of ovarian cancer. *Surg . Laparosc Endosc* 1996; **6**: 38–45.
11 Casey AC, Farias-Eisner R, Pisani AL et al. What is the role of reassessment laparoscopy in the management of gynecologic cancers in 1995? *Gynecol Oncol* 1996; **60**: 454–461.
12 Huang D, Swanson EA, Lin CP et al. Optical coherence tomography. *Science* 1991; **254**: 1178–1181.
13 Fujimoto JG, Brezinski ME, Tearney GJ et al. Biomedical imaging and optical biopsy using optical coherence tomography. *Nature Med* 1995; **1**: 970–972.
14 Puliafito CA, Hee MR, Lin CP et al. Imaging of macular diseases with optical coherence tomography. *Ophthalmol* 1995; **120**: 217–229.
15 Brezinski ME, Tearney GJ, Bouma BE et al. Optical coherence tomography for optical biopsy: properties and demonstration of vascular pathology. *Circulation* 1996; **93**: 1206–1213.
16 Schmitt JM, Yadlowsky MJ, Bonner RF. Subsurface imaging of living skin with optical coherence tomography. *Dermatology* 1995; **191**: 93–98.
17 Herrmann JM, Brezinski ME, Bouma BE et al. Two- and three-dimensional high-resolution imaging of the human oviduct with optical coherence tomography. *Fertil Steril* 1998; **70**: 155–158.
18 Boppart SA, Bouma BE, Pitris C et al. Intraoperative assessment of microsurgery with three-dimensional optical coherence tomography. *Radiology* 1998; **208**: 81–86.
19 Boppart SA, Brezinski ME, Pitris C, Fujimoto JG. Optical coherence tomography for neurosurgical imaging of human intracortical melanoma. *Neurosurgery* 1998; **43**: 834–841.
20 Tearney GJ, Brezinski ME, Bouma BE et al. *In vivo* endoscopic optical biopsy with optical coherence tomography. *Science* 1997; **276**: 2037–2039.
21 Boppart SA, Bouma BE, Pitris C, Tearney GJ, Brezinski ME, Fujimoto JG. Forward-imaging instruments for optical coherence tomographic imaging. *Opt Lett* 1997; **22**: 1618–1620.
22 Clivaz X, Marquis-Weible F, Salathe RP. Optical low coherence reflectometry with 1·9 μm spatial resolution. *Electron Lett* 1992; **28**: 1553–1555.
23 Bouma BE, Tearney GJ, Boppart SA, Hee MR, Brezinski ME, Fujimoto JG. High resolution optical coherence tomographic imaging using a modelocked Ti: Al_2O_3 laser. *Opt Lett* 1995; **20**: 1486–1488.
24 Boppart SA, Bouma BE, Pitris C, Southern JF, Brezinski ME, Fujimoto JG. *In vivo* cellular optical coherence tomography imaging. *Nature Med* 1998; **4**: 861–865.
25 Ramanujam N, Mitchell MF, Mahadevan A et al. In vivo diagnosis of cervical intraepithelial neoplasia using 337-nm-excited laser-induced fluorescence. *Proc Natl Acad Sci* 1994; **91**: 10193–10197.
26 Andrus PG, Strickland RD. Cancer grading by Fourier transform infrared spectroscopy. *Biospectroscopy* 1998; **4**: 37–46.

Accepted 12 May 1999